atmosphere

Article

The New Improved ZHD and Weighted Mean Temperature Models Based on GNSS and Radiosonde Data Using GPT3 and Fourier Function

Li Li [1,*], Ying Gao [2], Siyi Xu [1], Houxian Lu [1], Qimin He [1] and Hang Yu [1]

[1] Research Center of Beidou Navigation and Remote Sensing, Suzhou University of Science and Technology, Suzhou 215009, China
[2] School of Earth Sciences and Engineering, Hohai University, Nanjing 211100, China
* Correspondence: gszl.lili@usts.edu.cn

Abstract: Compared to the zenith hydrostatic delay (ZHD) obtained from the Saastamonien model based on in-situ measured meteorological (IMM) data and radiosonde-derived weighted mean temperature (T_m), the ZHD and T_m deviations of the GPT3 model have shown obvious periodic trends. This article analyzed the seasonal variations of GPT3-ZHD and GPT3-T_m during the 2016–2020 period in the Yangtze River Delta region, and the new improved ZHD and T_m models were established by the multi-order Fourier function. The precision of the improved-ZHD model was verified using IMM-ZHD products from 7 GNSS stations during the 2016–2020 period. Furthermore, the precisions of improved T_m and precipitable water vapor (PWV) were verified by radiosonde-derived T_m and PWV in the 2016–2019 period. Compared with the IMM-ZHD and GNSS-PWV products, the mean Bias and RMS of GPT3-ZHD are −0.5 mm and 2.1 mm, while those of GPT3-PWV are 2.7 mm and 11.1 mm. Compared to the radiosonde-derived T_m, the mean Bias and RMS of GPT3-T_m are −0.8 K and 3.2 K. The mean Bias and RMS of the improved-ZHD model from 2019 to 2020 are −0.1 mm and 0.5 mm, respectively, decreasing by 0.4 mm and 1.6 mm compared to the GPT3-ZHD, while those of the improved-T_m are −0.6 K and 2.7 K, respectively, decreasing by 0.2 K and 0.5 K compared to GPT3-T_m. The mean Bias and RMS of PWV calculated by GNSS-ZTD, improved-ZHD, and improved-T_m are 0.5 mm and 0.6 mm, respectively, compared to the GNSS-PWV, decreasing by 2.2 mm and 10.5 mm compared to the GPT3-PWV. It indicates that the improved ZHD and T_m models can be used to obtain the high-precision PWV. It can be applied effectively in the retrieval of high-precision PWV in real-time in the Yangtze River Delta region.

Keywords: GPT3; Fourier function; zenith hydrostatic delay (ZHD); weighted mean temperature (T_m); precipitable water vapor (PWV)

Citation: Li, L.; Gao, Y.; Xu, S.; Lu, H.; He, Q.; Yu, H. The New Improved ZHD and Weighted Mean Temperature Models Based on GNSS and Radiosonde Data Using GPT3 and Fourier Function. *Atmosphere* **2022**, *13*, 1648. https://doi.org/10.3390/atmos13101648

Academic Editors: Fei Yang, Lei Wang and Qingzhi Zhao

Received: 30 August 2022
Accepted: 6 October 2022
Published: 10 October 2022

1. Introduction

Sufficient atmospheric water vapor is one of the necessary conditions for precipitation formation, and water vapor detection plays an important role in weather forecasting, disaster monitoring and global climate change monitoring [1]. GNSS precipitable water vapor (GNSS-PWV) can be used to reflect the atmospheric water vapor variations in GNSS meteorology. It has the potential to forecast severe weather phenomena [2–4] and examine the effects of climate change [5,6]. Previous studies [3,7–10] have shown that there will be severe rainstorms in the downward trend process after GNSS-PWV reaches its peak value. Benevides et al. [11] proposed that the accuracy of weather forecasting could be improved after analyzing 3D distribution variations of PWV [12–16].

The inversion process of GNSS-PWV requires the zenith wet delay (ZWD) and the water vapor conversion coefficient (K). ZWD can be obtained by subtracting the zenith hydrostatic delay (ZHD) from the zenith total delay (ZTD) [17]. ZHD is the main delay for the GNSS signals transmitted in the neutral atmosphere, accounting for more than 90%

of ZTD. It means that the precision of ZHD will indirectly affect the precision of ZWD. The weighted mean temperature (T_m) is one of the important parameters to calculate K for the conversion of ZWD to PWV [18]. The ZHD and T_m play a crucial role in obtaining high-precision real-time GNSS-PWV [19,20].

Currently, the commonly used ZHD models can be divided into two categories. One is the empirical models based on the measured meteorological parameters, including the Saastamonien [21], Hopfield [22], and Black [23] models. For example, the Saastamonien model uses meteorological sensors to measure surface pressure and can calculate the ZHD at a millimeter level. However, it is difficult to obtain the measured meteorological parameters in real time at any place in the world, which limits the application of tropospheric delay models that need measured meteorological parameters with respect to GNSS meteorology. In this case, the use of atmospheric data to establish regional or global real-time tropospheric delay models has been widely concerned, such as UNB3m [24], EGNOS [1] and GPT [25–28]. ERA-Interim [29] and ERA5 [30] are also used to interpolate surface meteorological parameters at the GNSS stations. At the same time, a series of studies have achieved fruitful results in this research area. Ghaffari Razin and Voosoghi [31] use Bernese GNSS software and Saastamoinen model to calculate the ZTD and ZHD, then the ZWD obtained by subtracting the ZHD from the ZTD is modeled by two different machine learning methods, which can obtain PWV with high accuracy. A site-specific ZHD model was established by collecting an atmospheric vertical profile from radiosondes stations. It provides an error about 0.19 mm, which can be used to accurately estimate PWV [32]. Yang, et al. [33] analyzed the global performance of the three most commonly used ZHD models, the best temperature and pressure models were established by evaluating the influence of different modeling factors and the meteorological parameters estimated by the above-mentioned models. Based on the ERA5 reanalysis data of the European Centre for Medium-Range Weather Forecasts (ECMWF), Mateus, et al. [34] developed a one-hour global air pressure and temperature model (HGPT) to provide pressure, temperature, ZHD, and T_m. Climate studies, GNSS meteorology and other atmospheric research can significantly benefit from it.

The T_m is a necessary parameter to calculate the K value and plays a key role in atmospheric water vapor conversion. Among various T_m calculation methods, the accuracy of radiosonde-derived T_m is the highest, but it is difficult to popularize due to the spatiotemporal limitation of radiosondes [35–37]. Therefore, Bevis used the ground surface temperature (T_s) from the profiles of vapor partial pressure and dewpoint temperature of North American radiosondes over a two-year period to establish a global mean temperature model in 1992 (T_m = 0.72 T_s + 70.2) [38]. However, due to the influence of location, time, and other factors, the regional accuracy of Bevis model is inconsistent. In general, the systematic deviation is greater than 4.0 K, and even greater than 8.0 K in some areas [39,40]. When encountering bad weather, it may even lead to a significant deviation of GNSS-PWV [41,42]. Considering the linear relationship between T_m and T_s, many scholars have established different regional T_m models (RTM) based on local radiosondes [40,42–44]. The RTM established in Hong Kong can control the deviation within 4.0 K, which is superior to the Bevis model [45]. Singh, et al. [46] have found that the site specific T_m model is better than the developed regional T_m model and global model at New Delhi and Patiala. Elhaty, et al. [47] use radiosonde profiles from four stations situated in Egypt during 2015–2016 and Bevis linear regression method to develop a new T_m model. Several RTMs using one factor (T_s) have been established in China [45,48–50]. Li and Mao [48] deeply studied the monthly coefficient of RTM in eastern China. Guo, et al. [51] established a good annual single factor RTM model based on sounding data in the Yangtze River Delta region. Based on the above research, the researchers established many multi-factor RTM models [52–54]. Considering the influence of pressure (P_s) and water vapor pressure (e_s) on T_m, Gong [52] analyzed the relationship between meteorological elements using the data of 123 radiosonde stations in China, and established multi-factor models in different climatic regions, effectively improving the accuracy of single factor models. However, the models established by Wang, Song, Dai, and Cao [53] show that there is little difference in accuracy between the single factor model and the multi-factor model in Hong Kong. According to the above linear regression models, the precision of non-linear RTM between T_m and T_s proposed and established by Yao, et al. [55], which is slightly better than that of linear RTM. Zhu, et al. [56] established a non-linear T_m model for China with elevation corrections, which provides a significant correction effect for T_m in the vertical direction. Lan, Zhang, and Geng [39] adopt the sliding average method to calculate the correlation coefficient between T_s of the ECMWF and T_m from the "GGOS Atmosphere". Compared to the T_m-T_s relation of Bevis model, the T_m Grid model shows higher precision. Most researchers will analyze its precision comparing the PWV calculated by different ZHD and T_m models [57,58].

As mentioned above, when GNSS stations lack meteorological instruments, GPT series models are usually used to obtain real-time meteorological parameters. Boehm, Heinkelmann and Schuh [25] first proposed GPT in 2007, which can provide the pressure and temperature at any geographical location on the earth surface. Lagler, Schindelegger, Böhm, Krásná, and Nilsson [28] developed the GPT2 by combining the GPT with global mapping function (GMF), which can provide more meteorological parameters. Böhm, Möller, Schindelegger, Pain and Weber [26] introduced the vertical gradient of water vapor pressure and T_m to establish GPT2w on the basis of GPT2 in 2015. The GPT3 model is the latest version of the GPT series models, it can provide not only parameters from GPT2w, but also empirical gradient grids and is one of the most accurate and widely used tropospheric delay models [27]. Many studies have shown that the GPT3 model can provide high-precision ZTD and horizontal gradient information on a global scale, however, due to the limitation of terrain and other conditions, the GPT3 model based on European Centre for Medium-Range Weather Forecasts (ECMWF) data cannot be perfectly applied to any area [59–61]. Therefore, in a specific time and area, the precision of GPT3 model may not meet the requirements of some high-precision GNSS-PWV applications

Based on the GNSS products and radiosondes data in the Yangtze River Delta region during the 2016–2020 period, this paper analyzed the seasonal variations of the T_m and ZHD of GPT3 model in the Section 2, and then the Fourier function was used to establish the improved ZHD and T_m models in the Section 3. Meanwhile, the precisions of these improved ZHD and T_m models were verified by comparing them with the GNSS and radiosondes products in the Section 3. The Section 4 is the conclusion.

2. Data Sources and Methodology

2.1. Data Sources

Data from seven GNSS stations in the Yangtze River Delta region from 2016 to 2020 [62], mainly including parameters such as altitude, pressure, temperature, ZTD, ZHD and PWV (time resolution is one hour) were used to analyze the precision of corresponding parameters from the GPT3 model. Among them, the deviation between GPT3-ZHD and IMM-ZHD during the 2016–2018 period was used to establish the improved-ZHD model based on the Fourier function, and IMM-ZHD from 2016 to 2020 was used to verify the precision of the improved-ZHD model.

Data from seven radiosonde stations in the Yangtze River Delta region from 2016 to 2019 were obtained from Wyoming State University (http://weather.uwyo.edu/upperair/sounding.html, accessed on 15 April 2022), and it include meteorological parameters such as pressure, temperature and elevation (time resolution is 12 h). The PWV and T_m can be obtained by the integration method, and used as a reference to analyze the precision of GPT3-T_m and its inversion precision of PWV. The deviation of the GPT3-T_m and the radiosonde-derived T_m obtained by the integration method during the 2016–2018 period was used to establish an improved T_m model based on the Fourier function, and the data from 2016 to 2019 were used to verify the precision of the improved T_m model. Figure 1 is the location information of 7 GNSS stations and seven radiosonde stations.

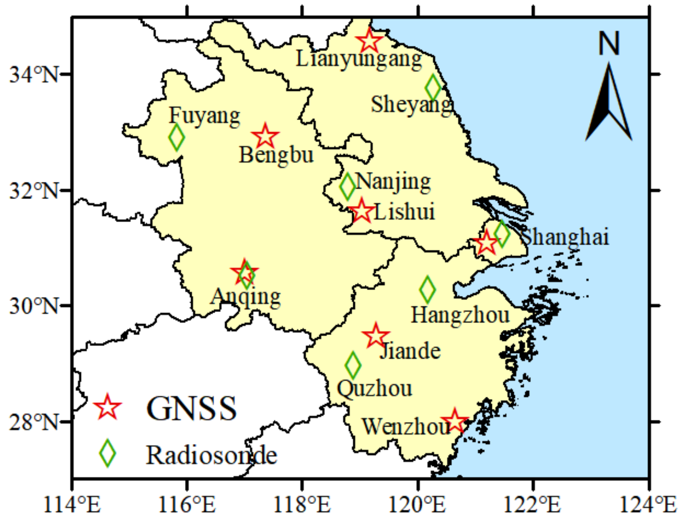

Figure 1. Distribution map of GNSS and radiosonde stations in the Yangtze River Delta region.

2.2. Methodology

2.2.1. T_m Calculation

The T_m is calculated by the numerical integration method using the radiosondes selected in Figure 1. The radiosonde-derived T_m has high calculation precision and is easy to realize [63]. It will be used as the reference or true value to evaluate the precision of GPT3-T_m.

$$\begin{cases} T_m = \frac{\int (e/T)dz}{\int (e/T^2)dz} \\ e = 6.112 \times e^{\frac{17.62t_d}{243.12+t_d}} \end{cases} \quad (1)$$

where, z is the elevation of the layer (km), e is the surface water vapor pressure (hPa), and t_d is the surface dew point temperature (°C).

2.2.2. GNSS-PWV and GPT3-PWV Calculations

GNSS has the advantages of all-weather, continuous and global coverage, it can provide high-precision ZTD except for navigation and positioning. According to the multi-frequency GNSS observations, the GNSS-ZTD time series can be obtained using precise point positioning (PPP) [64]. Firstly, the real-time clock error of satellites can be obtained by the data of GNSS reference stations and IGU orbit from IGS, then, then the time series of real-time ZTD will be calculated by the PPP routine of RTKLib on the basis of the real-time clock error of satellites and IGU products [3].

GNSS-ZTD consists of IMM-ZHD and GNSS-ZWD (ZTD = ZWD + ZHD), and the IMM-ZHD can be calculated by the Saastamonien model based on the latitude, air pressure and elevation of the sites [21], the formula is as follows.

$$\begin{cases} \mathrm{IMM-ZHD} = 0.0022768 \times \frac{P_c}{f(\varphi_c, H_c)} \\ f(\varphi_c, H_c) = 1 - 0.002\,66 \cos 2\varphi_c - 0.000\,28 H_c \end{cases} \quad (2)$$

where, P_c is the pressure of the station (hPa), φ_c is the latitude of the station (°), H_c is the elevation of the station (km). ZWD obtained by ZTD minus ZHD and the GNSS-PWV is determined by the following expression.

$$\begin{cases} \mathrm{PWV} = K \times \mathrm{ZWD} \\ K = \frac{10^5}{R_v\left(k_3/T_m + k_2'\right)} \end{cases} \quad (3)$$

where, K is the atmospheric water vapor conversion coefficient, R_v is the gas constant of the water vapor ratio, $R_v = 461\left(\mathrm{J{\cdot}K{\cdot}kg^{-1}}\right)$; k_2' and k_3 are the atmospheric refractive index constants; $K_3 = 3.776 \times 10^5 \left(\text{K}^2 \cdot \text{hpa}^{-1}\right)$; $k_2' = k_2 - k_1 \cdot (m_v/m_d) \left(\text{K} \cdot \text{hpa}^{-1}\right)$; $k_1 = 77.604$ (K·hPa); $k_2 = 64.79$ $(K \cdot \text{hPa})$; $m_v = 18.0152 \left(\text{g} \cdot \text{mol}^{-1}\right)$; $m_d = 28.9644 \left(g \cdot \text{mol}^{-1}\right)$; The T_m is obtained from the measured meteorological data according to Equation (1).

GPT3-PWV and GNSS-PWV adopt the same calculation method as Equation (3), but the difference is that T_m and ZWD for GPT3-PWV are obtained from the GPT3 model, which is more convenient.

2.2.3. Fourier Function

The Fourier function is a special triangular series proposed by Fourier, a French mathematician. Its characteristics and advantages are that complex functions can be transformed into linear combinations of simple trigonometric functions, which can accurately approximate any complex function, achieving the purpose of studying complex functions when given the appropriate orders, coefficients, and frequency [65]. The basic formula is as follows.

$$y = f(x) = a_0 + \sum_{n=0}^{m} (a_n \cos(n \times x \times w) + b_n \sin(n \times x \times w)) \tag{4}$$

where, m is the orders, w is the frequency, and a_n and b_n are the coefficients.

2.2.4. Statistical Method

The mean Bias and the root mean square (RMS) are used to evaluate the precision of the meteorological parameters and improved models as follows.

$$\begin{cases} \text{Bias} = \frac{\sum_{i=1}^{n}\left(x_{model,i} - x_{true,i}\right)}{n} \\ \text{RMS} = \sqrt{\frac{\sum_{i=1}^{n}\left(x_{model,i} - x_{true,i}\right)^2}{n}} \end{cases} \tag{5}$$

where, $X_{model,i}$ and $X_{true,i}$ represent parameter value of the models and truth, respectively, and the n is the number of samples.

3. Results and Discussions

The GPT series model (http://ggosatm.hg.tuwien.ac.at/DELAY/, accessed on 10 January 2022) is one of the popular open-source tropospheric delay models by adding empirical meteorological parameters. It only needs to provide the approximate coordinates of the station (Latitude, Longitude, Height) and day of year (DOY), and the values of meteorological parameter at any location all over the world can be obtained. The GPT3 model, as the latest model of the GPT series, has added gradients in two directions (N for north and E for east), and is completely consistent with the Vienna mapping function (VMF3), which can meet various purposes for meteorological and climate research. Its formula is as follows.

$$r(t) = A_0 + A_1 \cos\left(2\pi \frac{doy}{365.25}\right) + B_1 \sin\left(2\pi \frac{doy}{365.25}\right) + A_2 \cos\left(4\pi \frac{doy}{365.25}\right) + B_2 \sin\left(4\pi \frac{doy}{365.25}\right) \tag{6}$$

where, $r(t)$ are the values of the meteorological parameters at the grid point; A_0 is the mean value; (A_1, B_1), the amplitudes of the annual cycle; and (A_2, B_2), the amplitudes of the semi-annual cycle. Coefficients can be obtained by combining external grid files $(\text{gpt3}_1.\text{grd})$ with bilinear interpolation.

The GPT3 model uses the Saastamonien model to calculate ZHD as shown in Equation (1). The Asken&Nordiuss model [66] is used to calculate the ZWD. The GPT3 model also provides some empirical meteorological parameters that are inconvenient to measure directly. These meteorological parameters can be used to calculate GPT3-ZWD; the calculation formula of GPT3-PWV is the same as Equation (2).

3.1. The Improved ZHD Model

The comparison of GPT3-ZHD and IMM-ZHD of four GNSS stations at Anqing, Bengbu, Lishui and Lianyungang from 2016 to 2020 is shown in Figure 2. It can be seen that ZHD shows obvious seasonal periodical changes, and the overall trend of the two types of ZHD is similar. The ZHD value reaches the valley value in June, while it reaches its peak value in December. Affected by location and altitude, the peak value (or valley value) of ZHD at each station generally has a millimeter to centimeter deviation.

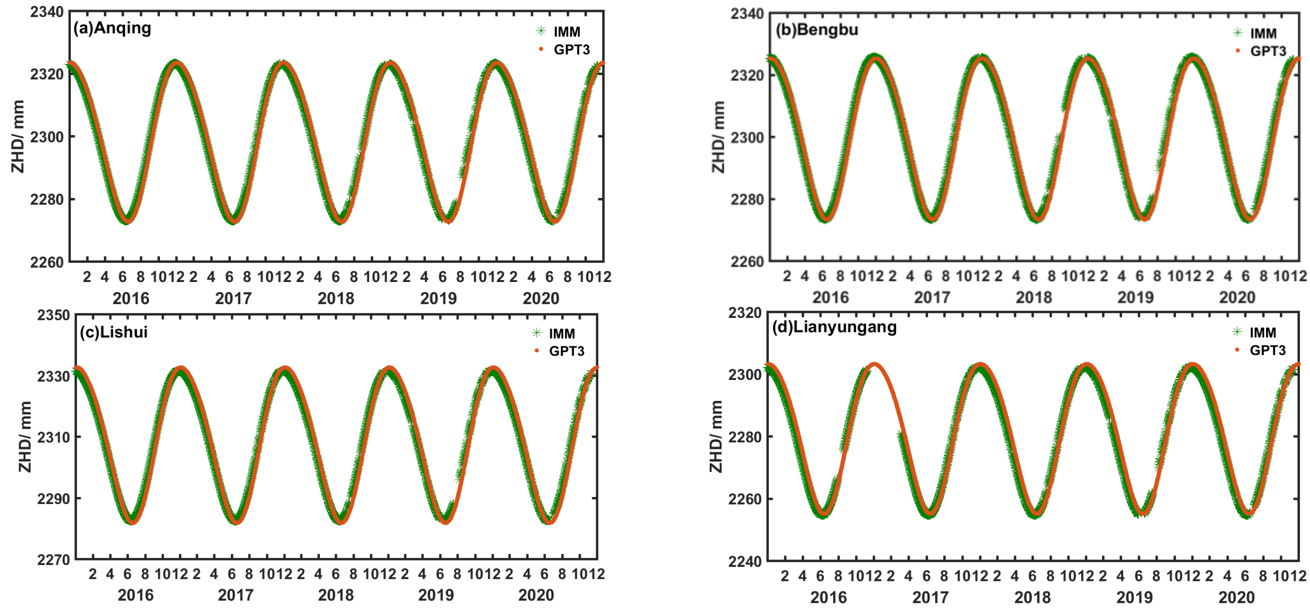

Figure 2. The seasonal variations of ZHD in Anqing (**a**), Bengbu (**b**), Lishui (**c**), and Lianyungang (**d**) during 2016–2020.

3.1.1. The Establishment of an Improved ZHD Model

Based on the analysis of GPT3-ZHD, experiments and analysis show that the Fourier function can be effectively used for model fitting. It will perform different fitting effects for the deviation of GPT3-ZHD by using different orders of the Fourier function. By comparison, the accuracy of the third order Fourier is much better than that of the first order, which is close to the fourth order, and the coefficient of the third order is simpler than that of the fourth order, so we chose the third order. Therefore, the third-order Fourier function is adopted to establish an improved ZHD model in this paper. Its calculation formula is as follows.

$$f(x) = a_0 + a_1 \cos xw + b_1 \sin xw + a_2 \cos 2xw + b_2 \sin 2xw + a_3 \cos 3xw + b_3 \sin 3xw \quad (7)$$

where, a_0, a_1, b_1, a_2, b_2, a_3, b_3, w, represent the coefficients, x is the day of year, and $f(x)$ is the deviation fitting curves based on the third-order Fourier function.

The GPT3-ZHD deviations of the 7 GNSS stations in the Yangtze River Delta region from 2016 to 2018 were used in Equation (7). It can obtain the model coefficients of the third-order Fourier function as shown in Table 1, which is a numerical description of the distribution characteristics of the GPT3-ZHD deviation. Figure 3 is the fitting curve of the ZHD deviation, it can be seen that the deviation distribution of GPT3-ZHD at seven stations is relatively small and the difference is mainly within 2 mm. The fitting curve agrees well with the deviation of each GNSS station, and the fitting deviation is mostly within 0.5 mm.

Table 1. The Fourier coefficients of the GPT3-ZHD bias in the Yangtze River Delta region during 2016–2018.

Parameter	a_0	a_1	b_1	a_2	b_2	a_3	b_3	w
ZHD	−0.3909	−0.2525	−2.676	−0.2953	0.3294	0.00059	−0.0097	0.01718

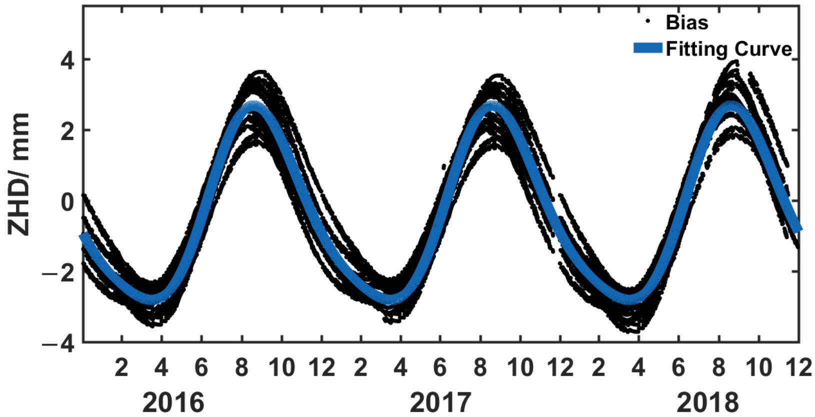

Figure 3. Bias and fitting curves of the GPT3-ZHD bias in the Yangtze River Delta region during 2016–2018.

3.1.2. Precision Analysis

The improved ZHD model established in the previous section can be used to predict the ZHD value (improved-ZHD) at GNSS stations from 2016 to 2020. Moreover, the article analyzed the precision of the improved ZHD model using the IMM-ZHD as the true value, and verified the weakening effect of the seasonal periodic deviation in Figure 4. It is clear that the periodic deviation of improved-ZHD at most stations has been greatly decreased, but the periodic fluctuation of improved-ZHD at Bengbu Station still has a small amplitude, which is related to the large gap between its GPT3-ZHD deviation and the overall trend of the deviation distribution. In general, most of the deviations of the improved ZHD model are maintained within 0.5 mm, and the precision of the improved-ZHD is greatly improved compared to the GPT3 model.

Table 2 shows the precision statistics of the improved ZHD model from 2016 to 2020. It can be seen from the table that the Bias and RMS of the improved ZHD model based on the Fourier function from 2019 to 2020 are −0.1 mm and 0.5 mm, respectively, which are 0.7 mm and 1.6 mm better than that of GPT3-ZHD, respectively. The overall precision of the improved-ZHD is significantly improved and relatively stable at each station. Therefore, the improved ZHD model has a higher precision and applicability than the GPT3 model in the Yangtze River Delta region.

3.2. The Improved T_m Model

Comparisons between the GPT3-T_m and the radiosonde-derived T_m (as a true value) at the four radiosondes in Anqing, Sheyang, Fuyang and Nanjing from 2016 to 2019 are shown in Figure 5. It can be seen that the T_m show obvious seasonal periodic changes and the overall change trends of the two types are similar, which are lower in spring and winter and higher in summer and autumn.

3.2.1. The Establishment of an Improved T_m Model

Based on the analysis of GPT3-T_m, the deviations of GPT3-T_m from seven radiosondes in the Yangtze River Delta region from 2016 to 2018 are substituted into Equation (7), and the coefficients of third order Fourier function model of GPT3-T_m deviations can be obtained as shown in Table 3.

Table 2. The precision of improved ZHD in the Yangtze River Delta region during the 2016–2020 period (mm).

Sites	GPT3-ZHD				Improved-ZHD			
	2016–2018		2019–2020		2016–2018		2019–2020	
	Bias	RMS	Bias	RMS	Bias	RMS	Bias	RMS
Anqing	−0.1	2.0	−0.2	2.1	0.3	0.4	0.4	0.4
Bengbu	0.1	2.2	−0.0	2.2	0.6	0.7	0.6	0.7
Jiande	−0.8	2.0	−1.0	1.8	−0.4	0.5	−0.4	0.7
Lishui	−0.2	2.1	−0.4	2.1	0.2	0.4	0.2	0.4
Lianyungang	−0.7	2.2	−1.0	2.3	−0.4	0.4	−0.4	0.4
Shanghai	−0.4	1.9	−2.2	2.3	0.0	0.4	−0.4	0.4
Wenzhou	−0.9	1.9	−1.0	2.0	−0.5	0.8	−0.4	0.5
Average	−0.4	2.0	−0.8	2.1	−0.0	0.5	−0.1	0.5

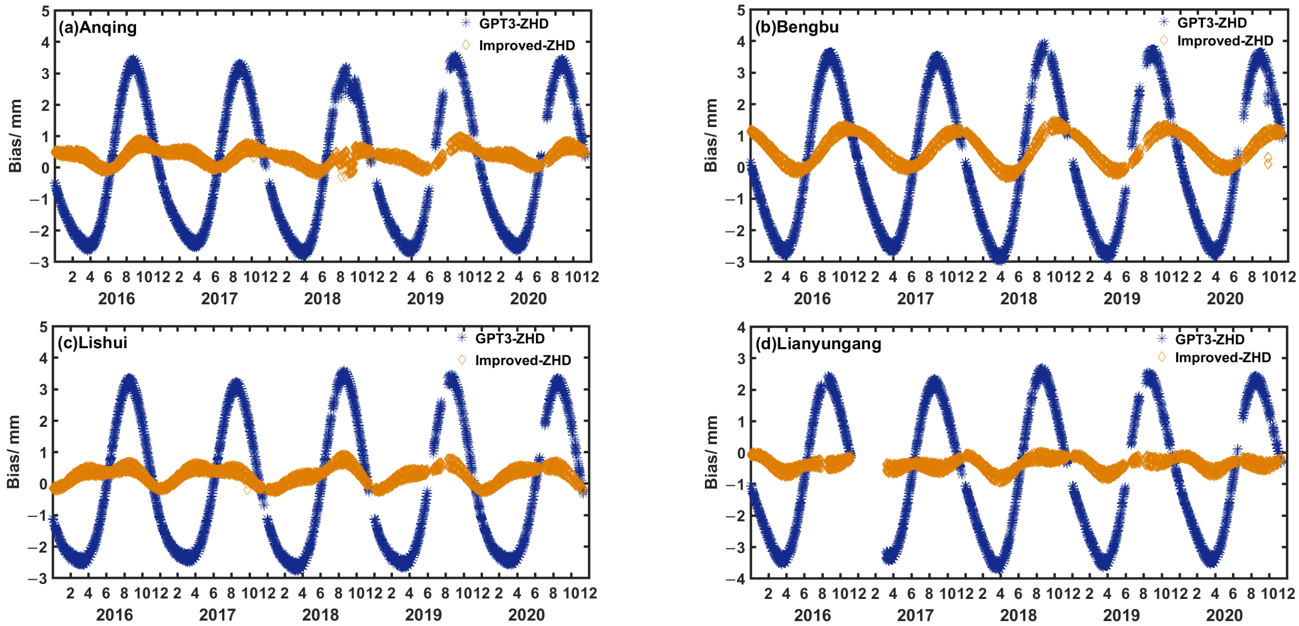

Figure 4. The bias of improved-ZHD and GPT3-ZHD at Anqing (**a**), Bengbu (**b**), Lishui (**c**), and Lianyungang (**d**) during the 2016–2020 period.

Table 3. Fourier coefficients of the GPT3-T_m bias in the Yangtze River Delta region during the 2016–2018 period.

Parameter	a_0	a_1	b_1	a_2	b_2	a_3	b_3	w
T_m	−0.8249	−1.247	1.301	−0.2511	−0.2311	0.2893	−0.9035	0.01729

The bias distribution of GPT3-T_m of the seven radiosondes is shown in Figure 6. It can be seen that the T_m deviations of nearly all radiosondes are maintained within ±10 K, but the deviation distribution is relatively discrete and exhibits obvious periodicity. A fitted curve has also been shown in the figure. It can describe the deviations distribution of GPT3-T_m well.

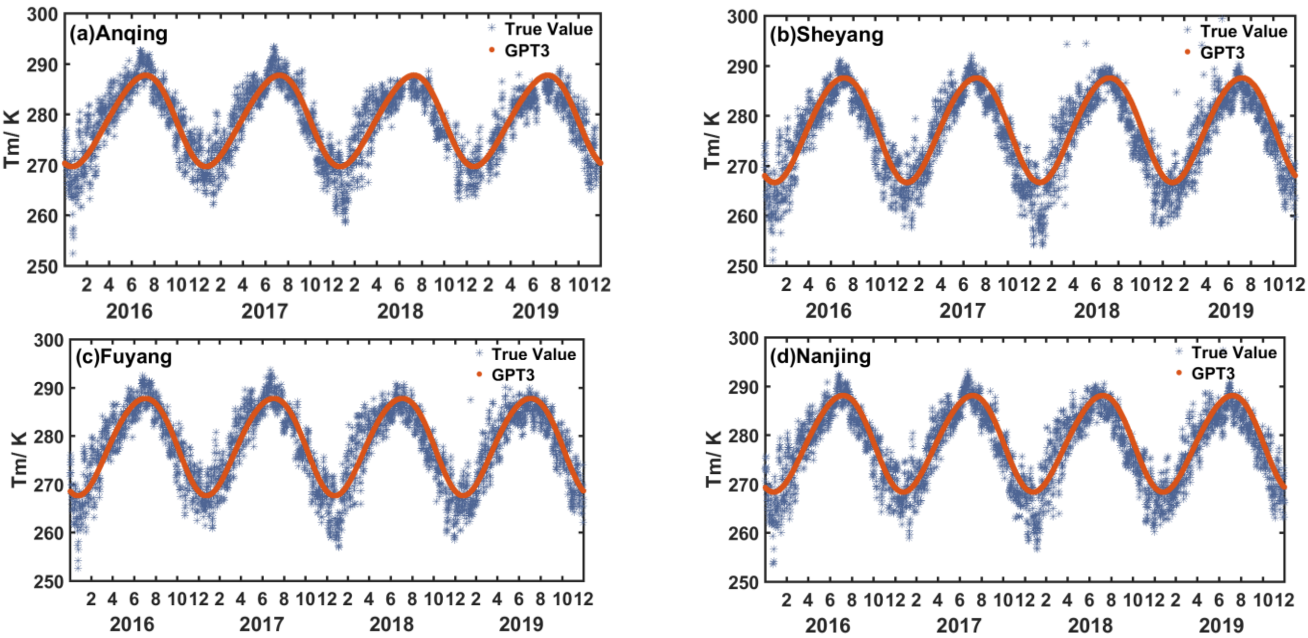

Figure 5. Variations of the GPT3-T_m in Anqing (**a**), Sheyang (**b**), Fuyang (**c**), and Nanjing (**d**) during the 2016–2019 period.

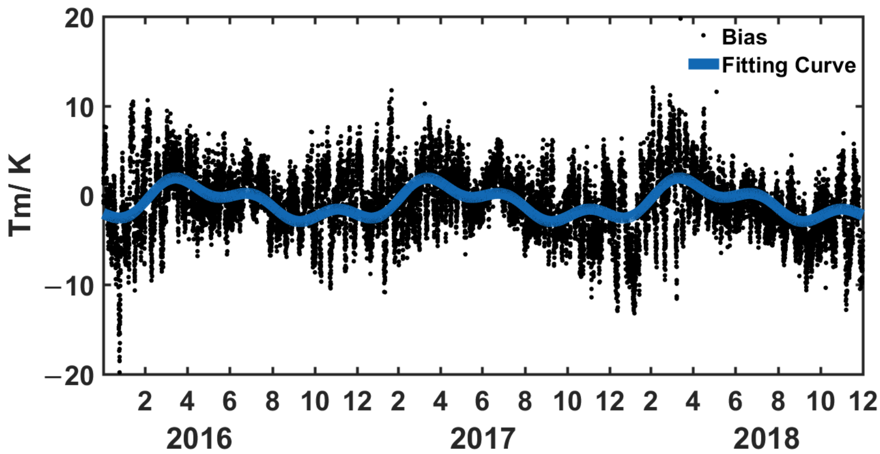

Figure 6. The bias and fitting curve of the GPT3-T_m in the Yangtze River Delta region during the 2016–2018 period.

3.2.2. Precision Analysis

The improved T_m model established in the previous section can be used to predict the T_m at seven radiosonde stations from 2016 to 2019. Furthermore, the article analyzed the precision of the improved T_m model using the radiosonde-derived T_m as true value, and verified the weakening effect of the seasonal periodic deviation of GPT3-T_m in Figure 7. It is clearly shown that the improved-T_m and GPT3-T_m are generally similar, and their deviations are both within $\pm$10 K compared to the radiosonde-derived T_m. However, the deviations of improved-T_m are more concentrated, indicating that the improvement effect is more obvious.

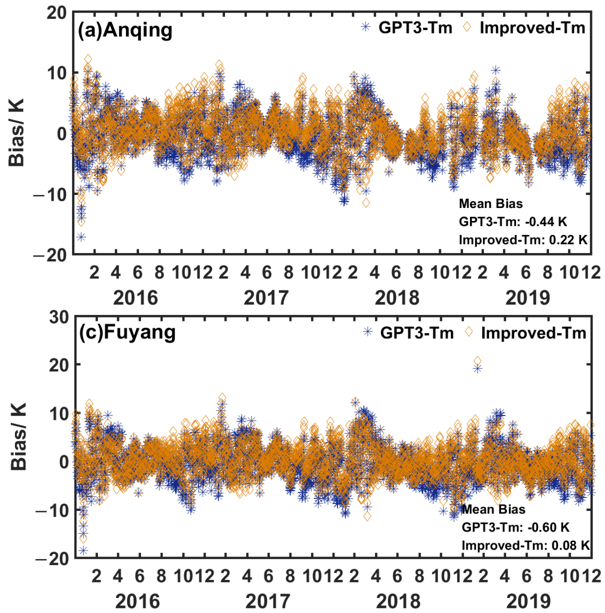

Figure 7. The bias of GPT3-T_m and improved-T_m in Anqing (**a**), Sheyang (**b**), Fuyang (**c**) and Nanjing (**d**) during the 2016–2019 period.

Table 4 is the precision statistics of the improved-T_m and the GPT3-T_m from 2016 to 2019. It can be seen that the mean Bias and RMS of improved-T_m are −0.6 K and 2.7 K in 2019, respectively, which are improved by 0.8 K and 0.4 K, respectively, compared to that of GPT3-T_m. Although the improvement of RMS is small, the bias of each station decreases steadily. Therefore, the improved T_m model in the paper has a higher and more stable precision than the GPT3 model in the Yangtze River Delta region.

Table 4. Precision of the GPT3-T_m and the improved-T_m in the Yangtze River Delta during the 2016–2019 period (K).

Sites	GPT3-T_m				Improved-T_m			
	2016–2018		2019		2016–2018		2019	
	Bias	RMS	Bias	RMS	Bias	RMS	Bias	RMS
Anqing	−0.2	3.0	−1.1	2.9	0.4	2.8	−0.3	2.7
Sheyang	−1.1	3.4	−1.7	3.3	−0.5	2.8	−0.9	2.7
Fuyang	−0.5	3.2	−1.0	2.9	0.2	2.9	−0.3	2.7
Nanjing	−0.8	3.2	−1.5	3.1	−0.2	2.8	−0.7	2.6
Hangzhou	−1.0	3.4	−1.8	3.4	−0.3	2.8	−1.0	2.8
Quzhou	0.1	3.0	−0.9	2.7	0.7	2.9	−0.2	2.5
Shanghai	−1.9	3.4	−1.9	3.4	−0.4	2.8	−1.1	2.6
Average	−0.8	3.2	−1.4	3.1	−0.0	2.8	−0.6	2.7

3.3. The PWV Based on Improved ZHD and T_m Models

The time series variation of GPT3-PWV and GNSS-PWV in Anqing (a), Bengbu (b), Lishui (c), and Lianyungang (d) during the 2016–2020 period is shown in Figure 8. Both GPT3-PWV and GNSS-PWV have obvious seasonal periodic changes, due to the influence of the subtropical monsoon in the Yangtze River Delta region, where rain and heat are in the same period, so the PWV is lower in spring and winter and higher in summer and autumn.

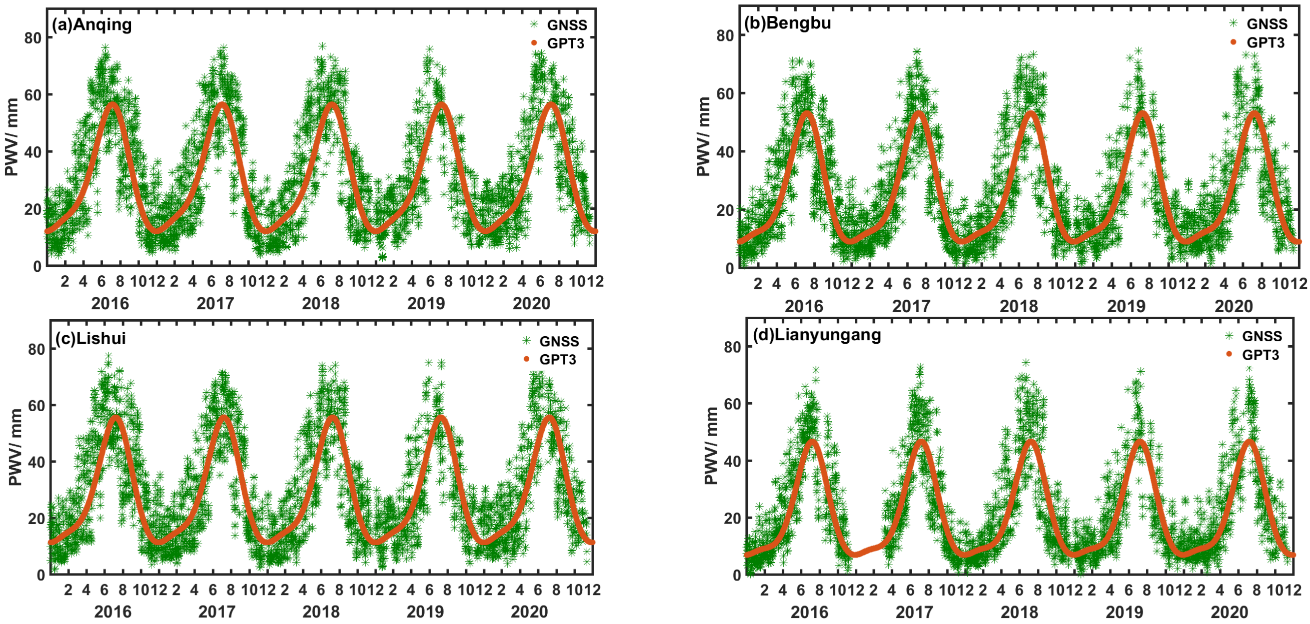

Figure 8. Time series variation of GPT3-PWV and GNSS-PWV in Anqing (**a**), Bengbu (**b**), Lishui (**c**), and Lianyungang (**d**) during 2016–2020.

GNSS-ZTD, improved-ZHD, and improved-T_m can be used integrated to calculate the improved-PWV at seven GNSS stations in the Yangtze River Delta region from 2016 to 2020 in the paper, the precision improvement of improved-PWV calculated as follows.

$$\begin{cases} \mathrm{PWV} = K \times (GNSS_{ZTD} - Improved_{ZHD}) \\ K = \dfrac{10^5}{R_v\left(k_3 / Improved_{Tm} + k_2'\right)} \end{cases} \tag{8}$$

where, $Improved_{Tm}$ and $Improved_{ZHD}$ come from the improved T_m and ZHD models based on Fourier functions in Sections 3.1 and 3.2. $GNSS_{ZTD}$ are obtained from GNSS, other parameters are the same as Equation (2).

The bias of GPT3-PWV and improved-PWV in Anqing (a), Bengbu (b), Lishui (c) and Lianyungang (d) during the 2016–2020 period is shown in Figure 9. The improved-PWV has greatly eliminated the seasonal periodic deviation of GPT3-PWV, indicating that the differences between the improved-PWV and GNSS-PWV are small and are highly consistent with each other.

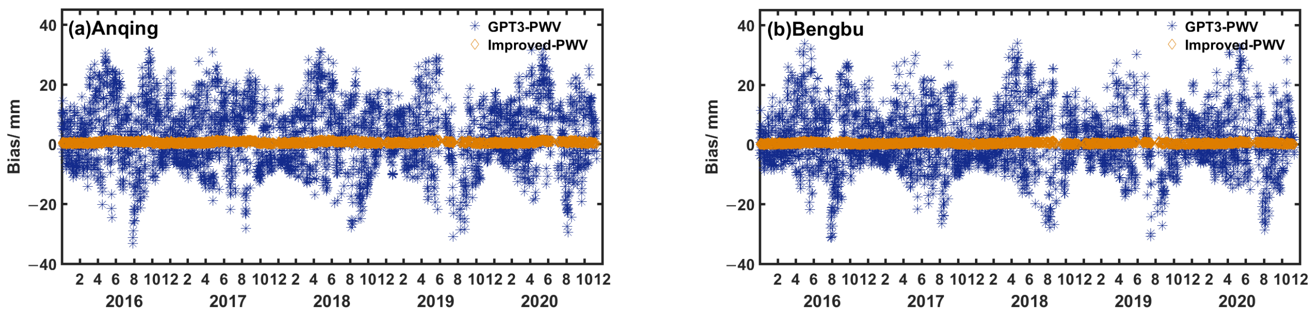

Figure 9. *Cont.*

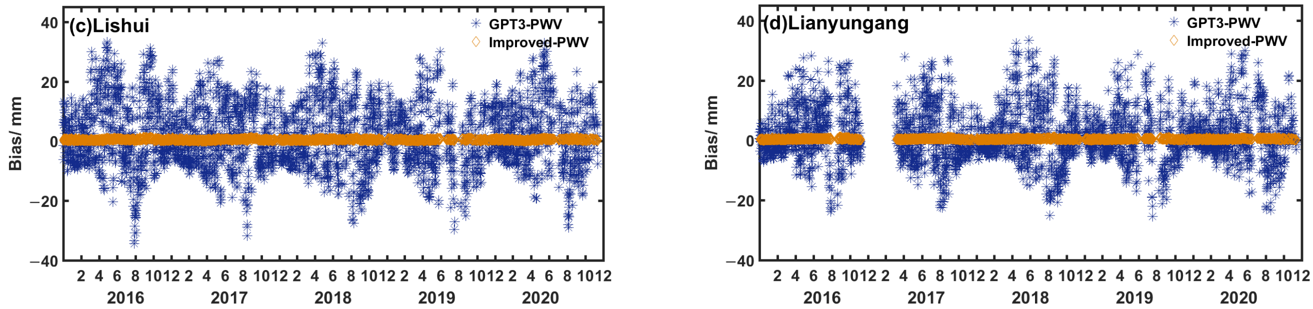

Figure 9. The bias of GPT3-PWV and improved-PWV in Anqing (**a**), Bengbu (**b**), Lishui (**c**), and Lianyungang (**d**) during the 2016–2020 period.

The precision statistics of GPT3-PWV and improved-PWV are shown in Table 5. It can be seen that the mean Bias and RMS of improved-PWV are 0.5 mm and 0.6 mm, respectively, which are 2.2 mm and 10.5 mm higher than that of GPT3-PWV, and the precision of GPT3-PWV is greatly improved. The precision of improved-PWV is very close to that of GNSS-PWV, and it can be used for real-time high-precision inversion of PWV in the Yangtze River Delta region.

Table 5. Precision of GPT3-PWV and improved-PWV in the Yangtze River Delta during 2016–2020 (mm).

Sites	GPT3-PWV		Improved-PWV	
	Bias	**RMS**	**Bias**	**RMS**
Anqing	2.9	11.3	0.6	0.6
Bengbu	1.3	10.2	0.5	0.6
Jiande	3.3	11.4	0.4	0.4
Lishui	1.8	11.2	0.5	0.5
Lianyungang	1.6	9.2	0.4	0.4
Shanghai	5.2	13.3	0.7	0.8
Wenzhou	3.0	11.0	0.7	0.7
Average	2.7	11.1	0.5	0.6

In order to further verify the inversion precision of improved-PWV, Anqing and Shanghai that have co-located radiosondes and GNSS stations are selected to compare improved-PWV and GNSS-PWV with radiosonde-derived PWV from 2016 to 2019. The bias of GNSS-PWV and improved-PWV is shown in Figure 10. The vacancy in the Figure 10b is caused by the lack of radiosonde and GNSS data after March 2019 in Shanghai station.

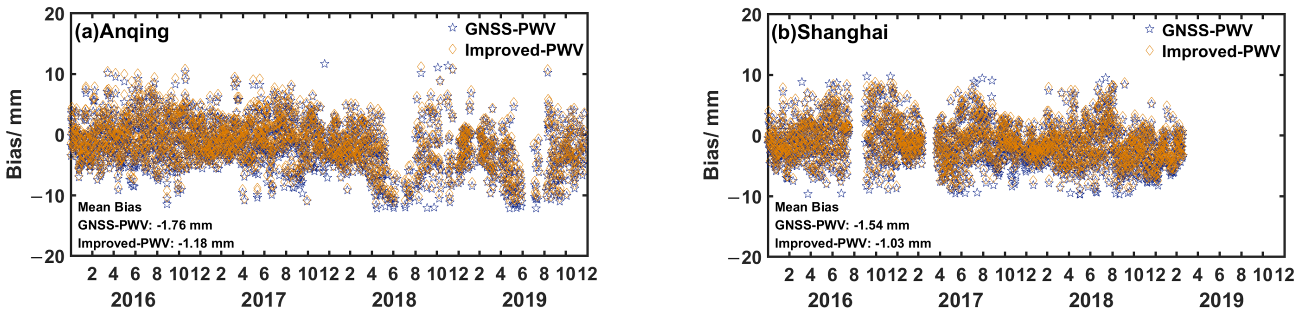

Figure 10. The bias of GNSS-PWV and improved-PWV in Anqing (**a**) and Shanghai (**b**) during the 2016–2019 period.

The deviation distribution of the improved-PWV and GNSS-PWV is in good agreement, and most deviations of the PWV are kept within ±10 mm, indicating that the precision of the improved-PWV and GNSS-PWV are equivalent.

Table 6 shows the precision statistics of improved-PWV and GNSS-PWV. Compared with the radiosonde-derived PWV, the mean Bias and RMS of the improved-PWV are −1.1 mm and 3.7 mm, respectively, which are 0.5 mm and 0.3 mm better than that of the GNSS-PWV, and the precision is slightly improved. It can be seen that the precision of PWV based on improved ZHD and T_m models is slightly better than that of GNSS-PWV, and they are roughly equivalent on the whole, which is further verified and demonstrated that the improved ZHD and T_m models can be used to obtain real-time high-precision PWV comparable to the GNSS-PWV precision.

Table 6. Precision of the GNSS-PWV and the improved-PWV at the co-located GNSS and radiosonde stations in Anqing and Shanghai during the 2016–2019 period (mm).

Sites	Improved-PWV		GNSS-PWV	
	Bias	RMS	Bias	RMS
Anqing	−1.2	3.9	−1.8	4.2
Shanghai	−1.0	3.4	−1.5	3.7
Average	−1.1	3.7	−1.6	4.0

4. Conclusions

The precision of the GPT3 model (ZHD, T_m and PWV) in the Yangtze River Delta region was first analyzed with reference to GNSS and radiosondes products. Aiming at the problem that the ZHD and T_m from GPT3 model have obvious seasonal periodic deviations, the third-order Fourier function was used to establish improved ZHD and T_m models, and their precision were analyzed and verified. The main research conclusions are as follows.

The mean biases of the GPT3-ZHD, T_m and PWV are −0.5 mm, −0.8 K, and 2.7 mm, respectively, and the mean RMS of those are 2.1 mm, 3.2 K, and 11.1 mm, respectively. Compared to the reference values of the GNSS products and radiosondes, the ZHD and PWV deviations have obvious seasonal variations. Specifically, the deviation of ZHD is negative in spring and winter, but positive in summer and autumn, and the deviation of PWV is smaller in spring and winter, but larger in summer and autumn.

Compare with the GPT3 model, the mean Bias and RMS of the improved-ZHD based on Fourier function from 2019 to 2020 are −0.1 mm and 0.5 mm, respectively, improved by 0.7 mm and 1.6 mm, while the mean Bias and RMS of the improved-T_m in 2019 are −0.6 K and 2.7 K, respectively, which are 0.8 K and 0.5 K better than GPT3-T_m. The precision of two models is improved slightly.

The mean Bias and RMS of the improved-PWV based on GNSS-ZTD and the improved ZHD and T_m models are 0.5 mm and 0.6 mm, respectively, which are 2.2 mm and 10.5 mm better than that of GPT3-PWV, and the overall precision is improved greatly. Compared to the radiosonde-derived PWV, the mean Bias and RMS are −1.1 mm and 3.7 mm, respectively, which are 0.5 mm and 0.3 mm higher than that of the GNSS-PWV, and the precision of the two methods performs similarly. Therefore, the improved ZHD and T_m models based on GPT3 and Fourier function established in the Yangtze River Delta region can be used for real-time high-precision PWV inversion.

Author Contributions: Conceptualization, L.L. and Y.G.; methodology, L.L.; software, S.X.; validation, S.X. and H.L.; formal analysis, Q.H.; investigation, Y.G.; resources, L.L.; data curation, S.X. and H.L.; writing—original draft preparation, L.L. and Y.G.; writing—review and editing, L.L. and Q.H.; visualization, Q.H. and H.Y.; supervision, L.L. and H.Y.; project administration, L.L. and H.Y.; funding acquisition, L.L. All authors have read and agreed to the published version of the manuscript.

Funding: This research was supported in part by the Strategic Priority Research Program of the Chinese Academy of Sciences (CAS) under Grant XDA17010304, the China Natural Science Funds under Grant 41904033, the CAS Pioneer Hundred Talents Program, the Natural Science Foundation of Hunan Province under Grant 2016JJ3061.

Institutional Review Board Statement: Not applicable.

Informed Consent Statement: Not applicable.

Data Availability Statement: Not applicable.

Acknowledgments: The authors would like to express their sincere gratitude to the University of Wyoming and Jiangsu Institute of Meteorological Sciences for the provision of radiosonde and GNSS observations. We also thank the reviewers for their constructive comments and suggestions, which resulted in a significant improvement in the quality of the paper.

Conflicts of Interest: The authors declare no conflict of interest.

References

1. Baker, H.C.; Dodson, A.H.; Penna, N.T.; Higgins, M.; Offiler, D. Ground-based GPS water vapour estimation: Potential for meteorological forecasting. *J. Atmos. Sol. Terr. Phys.* **2001**, *63*, 1305–1314. [CrossRef]
2. Iwabuchi, T.; Rocken, C.; Lukes, Z.; Mervart, L.; Johnson, J.; Kanzaki, M. PPP and Network True Real-time 30 sec Estimation of ZTD in Dense and Giant Regional GPS Network and the Application of ZTD for Nowcasting of Heavy Rainfall. In Proceedings of the ION GNSS 19th International Technical Meeting of the Satellite Division, Fort Worth, TX, USA, 26–29 September 2006; pp. 1902–1909.
3. Li, L.; Kuang, C.-L.; Zhu, J.-J.; Chen, W.; Chen, Y.-Q.; Long, S.-C.; Li, H.-Y. Rainstorm nowcasting based on GPS real-time precise point positioning technology. *Chin. J. Geophys.* **2012**, *55*, 1129–1136.
4. Li, H.; Wang, X.; Wu, S.; Zhang, K.; Chen, X.; Qiu, C.; Zhang, S.; Zhang, J.; Xie, M.; Li, L. Development of an Improved Model for Prediction of Short-Term Heavy Precipitation Based on GNSS-Derived PWV. *Remote Sens.* **2020**, *12*, 4101. [CrossRef]
5. Bianchi, C.E.; Mendoza, L.P.O.; Fernández, L.I.; Natali, M.P.; Meza, A.M.; Moirano, J.F. Multi-year GNSS monitoring of atmospheric IWV over Central and South America for climate studies. *Ann. Geophys.* **2016**, *34*, 623–639. [CrossRef]
6. Kruczyk, M. Long Series of GNSS Integrated Precipitable Water as a Climate Change Indicator. *Rep. Geod. Geoinform.* **2015**, *99*, 1–18. [CrossRef]
7. Wang, B.; Zhao, L.; Bai, X. The Characteristics Investigation of Ground-Based GPS/PWV During the "7.21" Extreme Rainfall Event in Beijing. In *China Satellite Navigation Conference (CSNC) 2015 Proceedings: Volume II*; Sun, J., Liu, J., Fan, S., Lu, X., Eds.; Lecture Notes in Electrical Engineering; Springer: Berlin/Heidelberg, Germany, 2015; Volume 341, pp. 563–574.
8. Simeonov, T.; Sidorov, D.; Teferle, F.N.; Milev, G.; Guerova, G. Evaluation of IWV from the numerical weather prediction WRF model with PPP GNSS processing for Bulgaria. *Atmos. Meas. Tech. Discuss.* **2016**, 1–15. [CrossRef]
9. Li, H.; Wang, X.; Choy, S.; Wu, S.; Jiang, C.; Zhang, J.; Qiu, C.; Li, L.; Zhang, K. A New Cumulative Anomaly-based Model for the Detection of Heavy Precipitation Using GNSS-derived Tropospheric Products. *IEEE Trans. Geosci. Remote Sens.* **2021**, *60*, 4105718. [CrossRef]
10. Li, H.; Wang, X.; Choy, S.; Jiang, C.; Wu, S.; Zhang, J.; Qiu, C.; Zhou, K.; Li, L.; Fu, E.; et al. Detecting heavy rainfall using anomaly-based percentile thresholds of predictors derived from GNSS-PWV. *Atmos. Res.* **2022**, *265*, 105912. [CrossRef]
11. Benevides, P.; Catalao, J.; Miranda, P.M.A. On the inclusion of GPS precipitable water vapour in the nowcasting of rainfall. *Nat. Hazards Earth Syst. Sci.* **2015**, *15*, 2605–2616. [CrossRef]
12. Jiang, P.; Ye, S.; Chen, D.; Liu, Y.; Xia, P. Retrieving Precipitable Water Vapor Data Using GPS Zenith Delays and Global Reanalysis Data in China. *Remote Sens.* **2016**, *8*, 389. [CrossRef]
13. Wang, H.; He, J.; Wei, M.; Zhang, Z. Synthesis Analysis of One Severe Convection Precipitation Event in Jiangsu Using Ground-Based GPS Technology. *Atmosphere* **2015**, *6*, 908–927. [CrossRef]
14. Song, D.-S.; Grejner-Brzezinska, D.A. Remote sensing of atmospheric water vapor variation from GPS measurements during a severe weather event. *Earth Planets Space* **2009**, *61*, 1117–1125. [CrossRef]
15. Manning, T.; Zhang, K.; Rohm, W.; Choy, S.; Hurter, F. Detecting Severe Weather using GPS Tomography: An Australian Case Study. *J. Glob. Position. Syst.* **2012**, *11*, 58–70. [CrossRef]
16. Zhang, K.; Manning, T.; Wu, S.; Rohm, W.; Silcock, D.; Choy, S. Capturing the Signature of Severe Weather Events in Australia Using GPS Measurements. *IEEE J. Sel. Top. Appl. Earth Obs. Remote Sens.* **2015**, *8*, 1839–1847. [CrossRef]
17. Huang, L.; Zhu, G.; Liu, L.; Chen, H.; Jiang, W. A global grid model for the correction of the vertical zenith total delay based on a sliding window algorithm. *GPS Solut.* **2021**, *25*, 98. [CrossRef]
18. Huang, L.; Peng, H.; Liu, L.; Xiong, S.; Xie, S.; Chen, J.; Li, J.; He, H. GNSS Precipitable Water Vapor Retrieval with the Aid of NWM Data for China. *Earth Space Sci.* **2021**, *8*, e2020EA001550. [CrossRef]
19. Wang, X.; Zhang, K.; Wu, S.; Fan, S.; Cheng, Y. Water vapor-weighted mean temperature and its impact on the determination of precipitable water vapor and its linear trend. *J. Geophys. Res. Atmos.* **2016**, *121*, 833–852. [CrossRef]
20. Li, L.; Wu, S.; Zhang, K.; Wang, X.; Li, W.; Shen, Z.; Zhu, D.; He, Q.; Wan, M. A new zenith hydrostatic delay model for real-time retrievals of GNSS-PWV. *Atmos. Meas. Tech.* **2021**, *14*, 6379–6394. [CrossRef]
21. Saastamoinen, J. Contributions to the theory of atmospheric refraction. *Bull. Géodésique* **1972**, *105*, 279–298. [CrossRef]
22. Hopfield, H.S. Tropospheric Effect on Electromagnetically Measured Range: Prediction from Surface Weather Data. *Radio Sci.* **1971**, *6*, 357–367. [CrossRef]

23. Black, H.D.; Eisner, A. Correcting satellite Doppler data for tropospheric effects. *J. Geophys. Res. Atmos.* **1984**, *89*, 2616–2626. [CrossRef]
24. Leandro, R.F.; Langley, R.B.; Santos, M.C. UNB3m_pack: A neutral atmosphere delay package for radiometric space techniques. *GPS Solut.* **2008**, *12*, 65–70. [CrossRef]
25. Boehm, J.; Heinkelmann, R.; Schuh, H. Short Note: A global model of pressure and temperature for geodetic applications. *J. Geod.* **2007**, *81*, 679–683. [CrossRef]
26. Böhm, J.; Möller, G.; Schindelegger, M.; Pain, G.; Weber, R. Development of an improved empirical model for slant delays in the troposphere (GPT2w). *GPS Solut.* **2015**, *19*, 433–441. [CrossRef]
27. Daniel, L.; Johannes, B. VMF3/GPT3: Refined discrete and empirical troposphere mapping functions. *J. Geod.* **2018**, *92*, 349–360.
28. Lagler, K.; Schindelegger, M.; Böhm, J.; Krásná, H.; Nilsson, T. GPT2: Empirical slant delay model for radio space geodetic techniques. *Geophys. Res. Lett.* **2013**, *40*, 1069–1073. [CrossRef]
29. Wang, X.; Zhang, K.; Wu, S.; He, C.; Cheng, Y.; Li, X. Determination of zenith hydrostatic delay and its impact on GNSS-derived integrated water vapor. *Atmos. Meas. Tech.* **2017**, *10*, 2807–2820. [CrossRef]
30. Zhang, W.; Zhang, H.; Liang, H.; Lou, Y.; Cai, Y.; Cao, Y.; Zhou, Y.; Liu, W. On the suitability of ERA5 in hourly GPS precipitable water vapor retrieval over China. *J. Geod.* **2019**, *93*, 1897–1909. [CrossRef]
31. Ghaffari Razin, M.-R.; Voosoghi, B. Modeling of precipitable water vapor from GPS observations using machine learning and tomography methods. *Adv. Space Res.* **2022**, *69*, 2671–2681. [CrossRef]
32. Singh, D.; Ghosh, J.; Kashyap, D. Development of a site-specific ZHD model using radiosonde data. *Acta Geod. Geophys. Hung.* **2012**, *47*, 90–100. [CrossRef]
33. Yang, F.; Meng, X.; Guo, J.; Shi, J.; An, X.; He, Q.; Zhou, L. The Influence of Different Modelling Factors on Global Temperature and Pressure Models and Their Performance in Different Zenith Hydrostatic Delay (ZHD) Models. *Remote Sens.* **2019**, *12*, 35. [CrossRef]
34. Mateus, P.; Catalão, J.; Mendes, V.B.; Nico, G. An ERA5-Based Hourly Global Pressure and Temperature (HGPT) Model. *Remote Sens.* **2020**, *12*, 1098. [CrossRef]
35. Bevis, M.; Businger, S.; Chiswell, S.; Herring, T.A.; Anthes, R.A.; Rocken, C.; Ware, R.H. GPS meteorology: Mapping zenith wet delays onto precipitable water. *J. Appl. Meteorol.* **1994**, *33*, 379–386. [CrossRef]
36. Hagemann, S.; Bengtsson, L.; Gendt, G. On the determination of atmospheric water vapor from GPS measurements. *J. Geophys. Res. Atmos.* **2003**, *108*, 4678. [CrossRef]
37. Huang, L.; Peng, H.; Liu, L.; Li, C.; Kang, C.; Xie, S. An empirical atmospheric weighted mean temperature model considering the lapse rate function for China. *Acta Geod. Cartogr. Sin.* **2020**, *49*, 432–442. [CrossRef]
38. Bevis, M.; Businger, S.; Herring, T.A.; Rocken, C.; Anthes, R.A.; Ware, R.H. GPS meteorology: Remote sensing of atmospheric water vapor using the global positioning system. *J. Geophys. Res. Atmos.* **1992**, *97*, 15787–15801.
39. Lan, Z.; Zhang, B.; Geng, Y. Establishment and analysis of global gridded Tm − Ts relationship model. *Geod. Geodyn.* **2016**, *7*, 101–102. [CrossRef]
40. Mircheva, B.R. Terrestrial Water Storage Anomaly during the 2007 Heat Wave in Bulgaria. Master's Thesis, Sofia University, Palo Alto, CA, USA, April 2016.
41. Basili, P.; Bonafoni, S.; Ferrara, R.; Ciotti, P.; Fionda, E.; Arnbrosini, R. Atmospheric water vapor retrieval by means of both a GPS network and a microwave radiometer during an experimental campaign in Cagliari, Italy, in 1999. *IEEE Trans. Geosci. Remote Sens.* **2001**, *39*, 2436–2443. [CrossRef]
42. Jiang, P.; Ye, S.R.; Liu, Y.Y.; Zhang, J.J.; Xia, P.F. Near real-time water vapor tomography using ground-based GPS and meteorological data: Long-term experiment in Hong Kong. *Ann. Geophys.* **2014**, *32*, 911–923. [CrossRef]
43. Song, D.-S.; Boutiouta, S. Determination of Algerian Weighted Mean Temperature Model for forthcoming GNSS Meteorology Application in Algeria. *J. Korean Soc. Surv. Geod. Photogramm. Cartogr.* **2012**, *30*, 615–622. [CrossRef]
44. Isioye, O.A.; Combrinck, L.; Botai, J. Modelling weighted mean temperature in the West African region: Implications for GNSS meteorology. *Meteorol. Appl.* **2016**, *23*, 614–632. [CrossRef]
45. Liu, Y.; Chen, Y.; Liu, J. Determination of weighted mean tropospheric temperature using ground meteorological measurements. *Geo-Spat. Inf. Sci.* **2001**, *4*, 14–18. [CrossRef]
46. Singh, D.; Ghosh, J.K.; Kashyap, D. Weighted mean temperature model for extra tropical region of India. *J. Atmos. Sol.-Terr. Phys.* **2014**, *107*, 48–53. [CrossRef]
47. Elhaty, N.M.; Abdelfatah, M.A.; Mousa, A.E.; El-Fiky, G.S. GNSS meteorology in Egypt: Modeling weighted mean temperature from radiosonde data. *Alex. Eng. J.* **2019**, *58*, 443–450. [CrossRef]
48. Li, J.; Mao, J. The approach to remote sensing of water vapor based on GPS and linear regression Tm in eastern region of China. *J. Meteorol. Res.* **1998**, *12*, 450–458.
49. Yu, S.; Liu, L. Validation and Analysis of the Water-Vapor-Weighted Mean Temperature from Tm-Ts Relationship. *Geomat. Inf. Sci. Wuhan Univ.* **2009**, *34*, 741–744.
50. Wang, Y.; Liu, L.; Hao, X.; Xiao, J.; Wang, H.; Xu, H. The application study of the GPS meteorology network in Wuhan region. *Acta Geod. Cartogr. Sin.* **2007**, *36*, 142–145.
51. Guo, B.; Li, L.; Xie, W. Modelling of weighted mean temperature using radiosonde data in Yangtze River Delta region. *J. Navig. Position.* **2019**, *7*, 61–67.

52. Gong, S. The Spatial and Temporal Variations of Weighted Mean Atmospheric Temperature and Its Models in China. *J. Appl. Meteorol. Sci.* **2013**, *24*, 332–334.
53. Wang, X.; Song, L.; Dai, Z.; Cao, Y. Feature analysis of weighted mean temperature Tm in Hong Kong. *J. Nanjing Univ. Inf. Sci.* **2011**, *3*, 47–52.
54. Yao, Y.; Zhang, B.; Xu, C.; Yan, F. Improved one/multi-parameter models that consider seasonal and geographic variations for estimating weighted mean temperature in ground-based GPS meteorology. *J. Geod.* **2013**, *88*, 273–282. [CrossRef]
55. Yao, Y.; Liu, J.; Zhang, B.; He, C. Nonlinear Relationships Between the Surface Temperature and the Weighted Mean Temperature. *Geomat. Inf. Sci. Wuhan Univ.* **2015**, *40*, 112–116.
56. Zhu, H.; Chen, K.; Huang, G. A Weighted Mean Temperature Model with Nonlinear Elevation Correction Using China as an Example. *Remote Sens.* **2021**, *13*, 3887. [CrossRef]
57. Ma, Y.; Chen, P.; Liu, T.; Xu, G.; Lu, Z. Development and Assessment of an ALLSSA-Based Atmospheric Weighted Mean Temperature Model with High Time Resolution for GNSS Precipitable Water Retrieval. *Earth Space Sci.* **2022**, *9*, e2021EA002089. [CrossRef]
58. Feng, P.; Li, F.; Yan, J.; Zhang, F.; JeanPierre, B. Assessment of the Accuracy of the Saastamoinen Model and VMF1/VMF3 Mapping Functions with Respect to Ray-Tracing from Radiosonde Data in the Framework of GNSS Meteorology. *Remote Sens.* **2020**, *12*, 3337. [CrossRef]
59. Yang, F.; Guo, J.; Zhang, C.; Li, Y.; Li, J. A Regional Zenith Tropospheric Delay (ZTD) Model Based on GPT3 and ANN. *Remote Sens.* **2021**, *13*, 838. [CrossRef]
60. Ding, J.; Chen, J. Assessment of Empirical Troposphere Model GPT3 Based on NGL's Global Troposphere Products. *Sensors* **2020**, *20*, 3631. [CrossRef]
61. Li, S.; Xu, T.; Xu, Y.; Jiang, N.; Bastos, L. Forecasting GNSS Zenith Troposphere Delay by Improving GPT3 Model with Machine Learning in Antarctica. *Atmosphere* **2022**, *13*, 78. [CrossRef]
62. Yu, J.; Tan, K.; Zhang, C.; Zhao, B.; Wang, D.; Li, Q. Present-day crustal movement of the Chinese mainland based on Global Navigation Satellite System data from 1998 to 2018. *Adv. Space Res.* **2019**, *63*, 840–856. [CrossRef]
63. Li, L.; Yuan, L.; Qimin, H.; Xiaoming, W. Weighted Mean Temperature Modelling Using Regional Radiosonde Observations for the Yangtze River Delta Region in China. *Remote Sens.* **2022**, *14*, 1909. [CrossRef]
64. Wang, K.; Khodabandeh, A.; Teunissen, P.J.G. MSE-impact of PPP-RTK ZTD estimation strategies. *Adv. Space Res.* **2018**, *61*, 2955–2971. [CrossRef]
65. Salcedo, A.C.; Recio, J.B. Fourier analysis of meteorological data to obtain a typical annual time function. *Sol. Energy* **1984**, *32*, 479–488. [CrossRef]
66. Askne, J.; Nordius, H. Estimation of tropospheric delay for microwaves from surface weather data. *Radio Sci.* **1987**, *22*, 379–386. [CrossRef]